Journal of Engineering Mathematics **36:** 241–254, 1999.

Airflow and temperature distribution in two-dimensional drying bins

W. PENG*, E. A. SMITH and A. de VILLE
Department of Mathematics and Statistics, University of Paisley, High Street PA1 2BE, Scotland, UK
e-mail: w.peng@bris.ac.uk.

Received 11 June 1996; accepted in revised form 8 December 1998

Abstract. The design of a drying or cooling store aims to provide an even airflow distribution, when aerated, for preservation purposes. The airflow in some curved bottom bins are studied in this paper. The flow is modelled, using Darcy's law. A generalized Schwarz-Christoffel transformation is employed to reduce the problem of computing streamlines and isobars of airflow to solving a single nonlinear equation for the flow angle along the wall. Corresponding to different bin shapes, a few computed streamlines and isobars of airflow are presented, showing the effect of changing bottom geometries on the air flow. Heat transfer in such bins is also investigated. Based on an analysis of the far field of airflow, finite-height bins are considered. Analytical solutions of the heat conduction equation in terms of streamlines and isobars are obtained.

Key words: flows in porous media, transformation, heat transfer, drying bins, conformal mapping.

1. Introduction

Bulk seed and cereal grain in store often require to be aerated for preservation purposes. Excess moisture in the grain can lead to the growth of mould which reduces grain quality. Various types of stores and driers are used for storage and drying systems. This paper is concerned with modelling the flow of air through the grain store, where the grain is treated as a porous medium. Similar drying systems are common throughout the food and chemical industries.

In practice, the damp cereal first needs to be dried by heated air to drive away the water content in the grain. This involves the transfer of moisture from the grain to the humid air, and hence the density of the air will change during this grain-drying process. The dried grain is then stored in the aerated bins. However, in this work, we consider the preservation of grain and study the air flows in the bins. Since the change of the density of the air becomes very small at this stage, we idealise the problem by ignoring the interaction between moist grain and humid air and treat the air density as constant, as a first step in the mathematical modelling.

If the velocity of the air flow is low enough, then Darcy's law is valid and the air pressure satisfies Laplace's equation, which can be solved by a range of analytical techniques. For examples, Spencer [1] used conformal mapping in estimating the pressure drop in the on-the-floor drying systems. In the case of a single duct, his method gave reasonable agreement with experiments. Hunter [2] studied two-dimensional flows in a semi-infinite bin also, using complex-variable techniques. Goudie *et al.* [3] considered a finite rectangular bin and they

* Present address: School of Mathematics, University of Bristol, University Walk, Bristol BS8 1TW, U.K.

obtained an analytic solution of flows in the bin, using the same complex-variable methods as Hunter did. They also studied the nonlinear Ergun equation, using a perturbation method. A more comprehensive numerical method is developed in the more recent work of Smith [4]. However, the thermal effect of the aerated air plays an important role in keeping the grain dry and driving away the moist air. But the study of the temperature distribution was ignored in all above mentioned work.

The problem will idealized two-dimensional bins with sharp corners is that flows pass through the region near a sharp corner very slowly and often leave part of the grain undried. In this study, we develop a scheme that we apply smoother wall shapes. Bins with curved walls are therefore treated, using a generalised Schwarz-Christoffel transformation. This allows a semi-analytic approach to the problem. An integral equation for the flow angles is obtained, which requires, in general, a numerical solution. After this integral equation is solved, the airflow distribution is computed. Some examples are provided to illustrate the numerical work. Based on fluid-flow results, the temperature field is approximated analytically. The method presented here provides an interesting alternative to the finite-element method.

Throughout this work the air flow is modelled, using Darcy's law and the flow is assumed to be incompressible. This gives a potential flow. In general the nonlinear Ergun equation [5] is used, but for low air velocity, such as in the range $0{\cdot}0017\,\mathrm{ms}^{-1} - 0{\cdot}08\,\mathrm{ms}^{-1}$ where the lower limit is obtained from the booklet [6], numerical results show that Darcy's model is to be within 1% of the nonlinear solution [4]. The formulation presented in this paper provides a way of studying the effect of altering the boundary shape on the streamlines and isobars. This, in turn, will alter the rate at which the grain is dried. An interesting problem is to find the shape which minimizes the drying time, though this problem is not tackled here.

Since the convective effect is important in this process, the heat-transfer equation is coupled with the flow velocity. To solve this equation, we transform the independent variables in the physical plane into the complex potential plane. The heat-transfer equation is reduced to a simple form which admits the standard techniques to find analytical solutions. An approximate solution will be presented in terms of the isobars and streamlines of the flow.

The rest of this paper is organized as follows; in Section 2, the mathematical model of the heated air flow issuing from a source is formulated. A transformation mapping the physical region onto an upper-half plane is made in Section 3. This mapping allows us to develop a numerical scheme applied for all kinds of different walls shapes. In Section 4, a few examples are provided to illustrate the method to get analytical and numerical results. The asymptotic analysis and a numerical scheme are provided in Section 5. The temperature distributions for finite-height bins are obtained in Section 6, with concluding remarks given in Section 7.

2. Mathematical formulations

The drying system is idealized as a two-dimensional bin, as shown in Figure 1. A steady, irrotational and incompressible air flow issuing from a source with strength Q and constant temperature T_0 inside a symmetric bin is considered. A Cartesian coordinate system is introduced with its origin at the bottom of the bin and $\tilde{y}$-axis vertically upwards, as shown in Figure 1(a). The bin consists of $\tilde{y} = f(\tilde{x})$ on $\tilde{y} < H$ and $\tilde{x} = \pm L$ on $\tilde{y} \geqslant H$. A typical velocity of the flow is given by $U = Q/(2L)$. The momentum equation is governed by Darcy's law

$$-\tilde{\nabla} P = \frac{\mu}{k}\tilde{\mathbf{u}}, \tag{2.1}$$

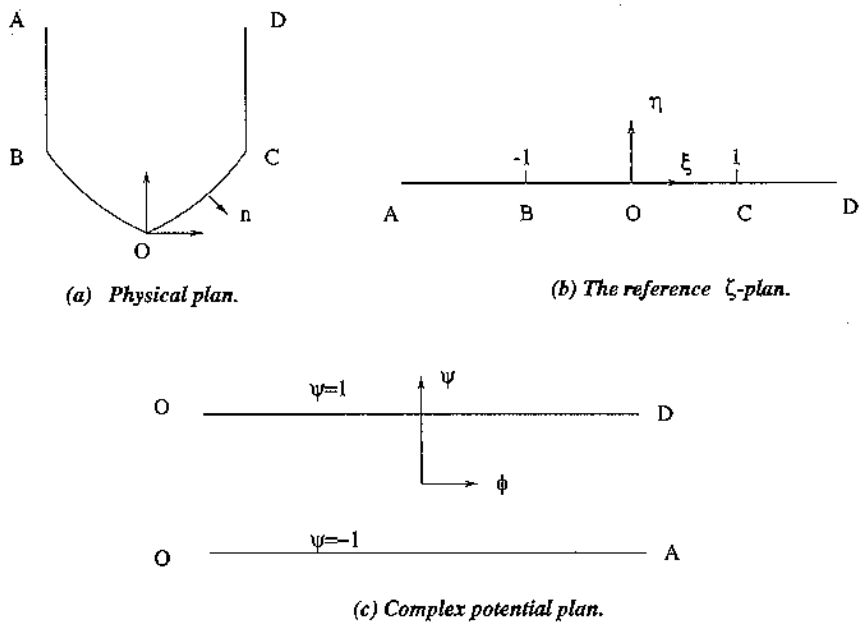

Figure 1. (a) Physical plane. (b) Reference plane $\zeta = \xi + i\eta$. (c) Complex potential plan.

where $\tilde{\nabla} = (\partial/\partial\tilde{x}, \partial/\partial\tilde{y})$, P is pressure, $\tilde{\mathbf{u}} = (\tilde{u}, \tilde{v})$ is velocity of air flow, viscosity μ and permeability k. The heat-transfer equation is

$$\tilde{u}\frac{\partial\tilde{T}}{\partial\tilde{x}} + \tilde{v}\frac{\partial\tilde{T}}{\partial\tilde{y}} = \frac{\tilde{K}}{\rho C}\nabla^2\tilde{T}, \tag{2.2}$$

where C is the heat capacity per unit mass, $\tilde{K} = n\lambda_f + (1-n)\lambda_s$($n$ is the porosity, λ_f the thermal conductivity of the fluid and λ_s the thermal conductivity of grains) represents the thermal conductivity and ρ is density of fluid. For air, we have $C = 1000\,\mathrm{J\,kg^{-1}\,K^{-1}}$, $\tilde{K}$ is within the range $0{\cdot}024 - 0{\cdot}031(\mathrm{Js^{-1}\,m^{-1}})$ for the temperature from 272 K to 373 K and $\rho = 1{\cdot}2\,\mathrm{kgm^{-3}}$.

The continuity equation is

$$\tilde{\nabla}\cdot\tilde{\mathbf{u}} = 0. \tag{2.3}$$

A complex variable $\tilde{z} = \tilde{x} + i\tilde{y}$ is introduced. The complex potential $W(\tilde{z}) = \Phi + i\Psi$ is also introduced, where Φ is the velocity potential and Ψ is the stream function. Nondimensionalization is given by means of transformations

$$z = x + iy = \frac{\tilde{z}}{L}, \qquad w = \phi + i\psi = \frac{W}{Q}, \qquad \frac{\tilde{u} + i\tilde{v}}{U} = u + iv, \tag{2.4}$$

$$p = \frac{kP}{\mu U}, \qquad \frac{\tilde{T} - T_1}{T_0 - T_1} = T. \tag{2.5}$$

Substituting these transformations in Equations (2.1), (2.2) and (2.3) yields

$$-\nabla p = \mathbf{u}, \tag{2.6}$$

$$u\frac{\partial T}{\partial x} + v\frac{\partial T}{\partial y} = \frac{1}{\mathrm{Pe}}\left(\frac{\partial T^2}{\partial x^2} + \frac{\partial T^2}{\partial y^2}\right), \tag{2.7}$$

$$\nabla \cdot \mathbf{u} = 0, \tag{2.8}$$

$$\mathbf{u}\cdot\mathbf{n} = 0, \qquad \mathbf{n}\cdot\nabla\mathbf{T} = \frac{\partial \mathbf{T}}{\partial \mathbf{n}} = \mathbf{0}, \qquad \psi = \pm\mathbf{1}, \tag{2.9}$$

where $\mathbf{n}$ is the outer normal vector, $\mathrm{Pe} = \rho C\, LU/\tilde{K}$, in Equation (2.7), is the Peclet number, and Equation (2.6) indicates $p = -\phi$. The boundary conditions in (2.9) state that the wall is impermeable for the fluid flow and that there is no heat exchange through the wall. Other temperature boundary conditions, for instance $T = 1$ on $\psi = \pm 1$, are also considered in this paper. If the boundary shape is unknown but the velocity distribution can be specified as constants on the boundaries of the curved portions and the contraction ratio is given, the boundary profile can be found by the use of the Schwarz-Christoffel transformation and the hodograph method. This idea has been developed and used in the design of wind tunnel contraction for incompressible invisid flow [7, 8].

3. Transformation of the physical plane

To transform the physical plane onto the upper half plane, we used a generalized Schwarz-Christoffel formula [9, pp. 163–175]. The transformation is given by

$$\frac{\mathrm{d}z}{\mathrm{d}\tilde{\zeta}} = M\exp\left\{-\frac{1}{\pi}\int_{-\infty}^{+\infty}\log(\tilde{\zeta}-t)\,\mathrm{d}\tilde{\theta}(t)\right\}, \tag{3.1}$$

where M is a constant and $\tilde{\theta}(t)$ is understood to be the tangential angle made by a smooth curve in the z-plane at the point which corresponds to $\tilde{\zeta} = t + i0$. This formula has been used some time ago to study the free-surface flows by Bloor [10] and King and Bloor [11]. Equation (3.1) can be written as

$$\frac{\mathrm{d}z}{\mathrm{d}\tilde{\zeta}} = M\exp\left\{-\frac{1}{\pi}\int_{-l}^{l}\log(\tilde{\zeta}-t)\,\mathrm{d}\tilde{\theta}(t) - \frac{\alpha}{\pi}\log(\tilde{\zeta}+l)(\tilde{\zeta}-l)\right\}, \tag{3.2}$$

where $2l$ corresponds to the distance BC in the upper half plane, the reference plane. Integrating by parts in Equation (3.2), we have

$$\begin{aligned}\frac{\mathrm{d}z}{\mathrm{d}\tilde{\zeta}} &= M\exp\left\{-\frac{1}{\pi}\left[\left(\frac{\pi}{2}-\alpha\right)\log(\tilde{\zeta}^2-l^2) + \int_{-l}^{l}\frac{\tilde{\theta}(t)}{\tilde{\zeta}-t}\,\mathrm{d}t + \alpha\log(\tilde{\zeta}+l)(\tilde{\zeta}-l)\right]\right\}\\ &= M(\tilde{\zeta}^2-l^2)^{-\frac{1}{2}}\exp\left\{-\frac{1}{\pi}\int_{-l}^{l}\frac{\tilde{\theta}(t)}{\tilde{\zeta}-t}\,\mathrm{d}t\right\},\end{aligned} \tag{3.3}$$

and introducing $\zeta = \tilde{\zeta}/l$ into Equation (3.3) we obtain

$$\frac{\mathrm{d}z}{\mathrm{d}\zeta} = M(\zeta^2-1)^{-\frac{1}{2}}\exp\left\{-\frac{1}{\pi}\int_{-l}^{l}\frac{\theta(t)}{\zeta-t}\,\mathrm{d}t\right\}, \tag{3.4}$$

where $\theta(t) = \tilde{\theta}(lt)$. The physical plane is then mapped into the upper half plane, as shown in Figure 1.

The constant M can be determined if we consider

$$(\zeta^2 - 1)^{-\frac{1}{2}} \exp\left\{-\frac{1}{\pi}\int_{-l}^{l} \frac{\theta(t)}{\zeta - t}\,\mathrm{d}t\right\} \sim \frac{1}{\zeta} \tag{3.5}$$

as $|\zeta| \to \infty$. From the width of the bin, we obtain

$$M = \frac{2i}{\pi},$$

so that (3.4) becomes

$$\frac{\mathrm{d}z}{\mathrm{d}\zeta} = \frac{2i}{\pi}(\zeta^2 - 1)^{-\frac{1}{2}} \exp\left\{-\frac{1}{\pi}\int_{-l}^{l} \frac{\theta(t)}{\zeta - t}\,\mathrm{d}t\right\}. \tag{3.6}$$

On the upper half $\zeta = \xi + i\eta$-plane, the complex potential for a point source can be readily written as

$$w = \phi + i\psi = \frac{2}{\pi}\log\zeta. \tag{3.7}$$

The velocity can be obtained from

$$\frac{\mathrm{d}w}{\mathrm{d}z} = \frac{\mathrm{d}w}{\mathrm{d}\zeta}\frac{\mathrm{d}\zeta}{\mathrm{d}z} = \frac{1}{2i}\frac{(\zeta^2 - 1)^{\frac{1}{2}}}{\zeta} \exp\left\{\frac{1}{\pi}\int_{-l}^{l} \frac{\theta(t)}{\zeta - t}\,\mathrm{d}t\right\}. \tag{3.8}$$

From Equations (3.6) and (3.8), we can see that once $\theta(\xi)$ has been found, the physical field and velocity field can be determined.

If the bottom shape of the bin is given by the function $y = f(x)$, then $\theta(\xi)$ satisfies the equation

$$\tan\theta(\xi) = f'\left(\int_0^{\xi} \frac{2}{\pi}\frac{\cos\theta(\xi)}{(1-\xi^2)^{\frac{1}{2}}} \exp\left\{-\frac{1}{\pi}\int_{-1}^{1} \frac{\theta(t)}{\xi - t}\,\mathrm{d}t\right\}\,\mathrm{d}\xi\right), \quad 0 < \xi < 1. \tag{3.9}$$

In general it is difficult to find an analytical solution to Equation (3.9). However, in some simple cases, solutions are obtained analytically, as shown in the following section.

4. Examples

Example 1. We first consider a bin with a flat bottom, *i.e.*, $\theta(t) = 0$, and Equation (3.6) then reduces to

$$\frac{\mathrm{d}z}{\mathrm{d}\zeta} = \frac{2}{\pi}(1 - \zeta^2)^{-\frac{1}{2}}, \tag{4.1}$$

which can be easily solved to obtain

$$z = \frac{2}{\pi}\arcsin\zeta. \tag{4.2}$$

After substituting (4.2) in (3.7), we have

$$w = \phi + i\psi = \frac{2}{\pi} \log \sin \frac{\pi z}{2}. \tag{4.3}$$

Therefore, we obtain

$$\frac{\mathrm{d}w}{\mathrm{d}z} = \frac{\cos \frac{\pi z}{2}}{\sin \frac{\pi z}{2}}. \tag{4.4}$$

This case has been discussed by Hunter [2] and Goudie *et al.* [3].

Example 2. For bins with cone bottom, for instance, $y = f(x) = |x|$, we obtain

$$\frac{\mathrm{d}z}{\mathrm{d}\zeta} = \frac{2i}{\pi}(\zeta - 1)^{-\frac{1}{4}} \zeta^{-\frac{1}{2}} (\zeta + 1)^{-\frac{1}{4}}. \tag{4.5}$$

Integrating this equation, we have

$$z = \frac{i}{\pi} \log \left[\frac{1 + i^{\frac{1}{2}} (\zeta^{-2} - 1)^{-\frac{1}{4}}}{1 - i^{\frac{1}{2}} (\zeta^{-2} - 1)^{-\frac{1}{4}}} \right] - i^{-\frac{1}{2}} \tan^{-1} i^{\frac{1}{2}} (\zeta^{-2} - 1)^{-\frac{1}{4}}. \tag{4.6}$$

Using $w = 2/\pi \log \zeta$, we obtain

$$\frac{\mathrm{d}w}{\mathrm{d}z} = -i\zeta^{-\frac{1}{2}} (\zeta^2 - 1)^{\frac{1}{4}}. \tag{4.7}$$

When the shape of the bin is a polygon, the transformation reduces to a Schwarz-Christoffel formula and we can obtain the solution by letting the flow angles be constants $\theta(\xi_i) = c_i (i = 1, \ldots, m)$, where m is the index of the sides of the polygon.

However, when the boundary is a continuous curve, a numerical scheme will have to be developed to solve (3.9). The flow pattern, velocity and therefore from Darcy's law, the pressure field will be obtained. The numerical scheme will be developed in next section. Since

$$\frac{\mathrm{d}z}{\mathrm{d}t} = \frac{\mathrm{d}w}{\mathrm{d}z}, \tag{4.8}$$

the fluid traverse time in the bin τ, is defined as

$$\tau = \int_0^x \frac{\mathrm{d}x}{V_x} = \int_0^y \frac{\mathrm{d}y}{V_y}. \tag{4.9}$$

It is thought that for low velocities, the traverse time gives a good estimate for the drying rate of grain (Hukill and Shedd [12] and Smith *et al.* [13]). Also, Equation (4.8) can be written as

$$\frac{\mathrm{d}t}{\mathrm{d}z} = \frac{\mathrm{d}z}{\mathrm{d}w}, \tag{4.10}$$

which reduces to

$$\tau = \int_0^z \frac{\mathrm{d}z}{\mathrm{d}w} \mathrm{d}z = \int_0^\zeta \left(\frac{\mathrm{d}z}{\mathrm{d}\zeta} \right)^2 \frac{\mathrm{d}\zeta}{\mathrm{d}w} \mathrm{d}\zeta. \tag{4.11}$$

Thus, for given $\zeta = \zeta_0$, seeking the best shape of the bin for minimum fluid traverse time turns to be looking for

$$t_0 = \mathrm{Min}_{\theta;\zeta} \left\{ -\int_0^{\zeta_0} \frac{4\zeta}{\pi(\zeta^2 - 1)} \exp\left\{ -\frac{2}{\pi} \int_{-1}^{1} \frac{\theta(t)}{\zeta - t}\, \mathrm{d}t \right\} \mathrm{d}\zeta \right\}.$$

We do not pursue this interesting problem any further here.

5. Asymptotic analysis and numerical scheme

We might expect changes in the bin bottom to only affect the flow field for small heights and to have little effect on the far field of flows. The asymptotic behaviour of the air flow far away from the bottom of the bin is investigated and the computational scheme for solving Equation (3.9) is explained. Equation (3.6) is rewritten as

$$\frac{\mathrm{d}z}{\mathrm{d}\zeta} = \frac{2}{\pi}(1 - \zeta^2)^{-\frac{1}{2}} N(\zeta), \tag{5.1}$$

where

$$N(\zeta) = \exp\left\{ -\frac{1}{\pi} \int_{-1}^{1} \frac{\theta(t)}{\zeta - t}\, \mathrm{d}t \right\}. \tag{5.2}$$

Integrating Equation (5.1) by parts we have

$$z - z_0 = \frac{2}{\pi} \left[N(\zeta) \arcsin \zeta - N(\zeta_0) \arcsin \zeta_0 - \int_{\zeta_0}^{\zeta} N'(\zeta) \arcsin \zeta \, \mathrm{d}\zeta \right]. \tag{5.3}$$

Since as $|\zeta| \to \infty$, $N(\zeta) \to 1$, hence

$$N'(\zeta) = N(\zeta) \frac{4\zeta}{\pi} \int_0^1 \frac{t\theta(t)}{(\zeta^2 - t^2)^2}\, \mathrm{d}t = O(\zeta^{-3})$$

and

$$\arcsin \zeta = -i \log(i\zeta \pm (1 - \zeta)^{\frac{1}{2}}) = O(\log \zeta).$$

Equation (5.3) yields

$$z - z_0 \sim \frac{2}{\pi} \arcsin \zeta - \arcsin \zeta_0 + F(\zeta_0) + O(\zeta^{-2} \log \zeta), \tag{5.4}$$

where

$$F(\zeta) = \int N'(\zeta) \arcsin \zeta \, \mathrm{d}\zeta.$$

The first term on the right-hand side of Equation (5.4) is the exact solution of the air flow in a rectangular bin. This dominates the behaviour of the upstream air flow for large ζ and shows

that varying the bottom shape of bin does not have a significant effect on the upstream air flow at large values of heights.

In order to solve Equation (3.9) numerically and to compute the streamlines and isobars from Equation (5.3), we introduce a complex variable as follows

$$u = u_1 + iu_2 = \frac{2}{\pi} \arcsin \zeta. \tag{5.5}$$

From Equation (3.7), the isobars and streamlines are then given by

$$\sin^2 \frac{\pi}{2} u_1 + \sinh^2 \frac{\pi}{2} u_2 C_1^2 \tag{5.6}$$

and

$$\tan \frac{\pi}{2} u_1 = C_2 \tanh \frac{\pi}{2} u_2, \tag{5.7}$$

respectively. Substituting (5.5) in (5.3) yields

$$z - z_0 = N\left(\sin \frac{\pi}{2} u\right) u - N\left(\sin \frac{\pi}{2} u_0\right) u_0 - \frac{\pi}{2} \int_{u_0}^{u} N'\left(\sin \frac{\pi}{2} t\right) t \cos \frac{\pi}{2} t \, \mathrm{d}t. \tag{5.8}$$

We take $y = x^2$ as an example to illustrate this scheme. The boundary Equation (3.9) in this case reduces to

$$\tan \theta(\xi) = \frac{4}{\pi} \int_0^{\xi} \frac{\cos \theta(\xi)}{(1-\xi^2)^{\frac{1}{2}}} \exp\left\{-\frac{1}{\pi} \int_{-1}^{1} \frac{\theta(t)}{\xi - t} \, \mathrm{d}t\right\} \, \mathrm{d}x. \tag{5.9}$$

Equation (5.9) is discretised, by means of the trapezoidal rule to obtain

$$\tan \theta(\xi_j) = \frac{4h}{\pi} \sum_{i=1}^{k} \frac{\cos \theta(\xi_i)}{(1-\xi_i^2)^{\frac{1}{2}}} N_i + O(h^2), \quad j = 1, \ldots, M \tag{5.10}$$

where

$$N_i = \exp\left\{-\frac{1}{\pi}\left[h \sum_{k=1, k\neq i}^{M} \frac{2\xi_k \theta(\theta_k)}{\xi_1^2 - \xi_k^2} + \int_{\xi_{i-1}}^{\xi_{i+1}} \frac{2t\theta(t)}{\xi_i^2 - t^2} \, \mathrm{d}t\right]\right\}. \tag{5.11}$$

The function $\theta(t)$ is expanded around ξ_i and the integral in the above equation can be evaluated as

$$\begin{aligned} \int_{\xi_{i-1}}^{\xi_{i+1}} \frac{2t\theta(t)}{\xi_i^2 - t^2} \, \mathrm{d}t \;=\; & -\theta(\xi_i) \log \frac{2\xi_i + h}{2\xi_i - h} \\ & -(\theta(\xi_{i+1}) - \theta(\xi_{i-1}))\left[1 - \frac{\xi_i}{h} \log \frac{2\xi_i + h}{2\xi_i - h}\right] + O(h^3). \end{aligned} \tag{5.12}$$

The equations in (5.10) form a system of M nonlinear equations of M variables, which is solved numerically by means of subroutine C05NBF in NAG library. The programme is run

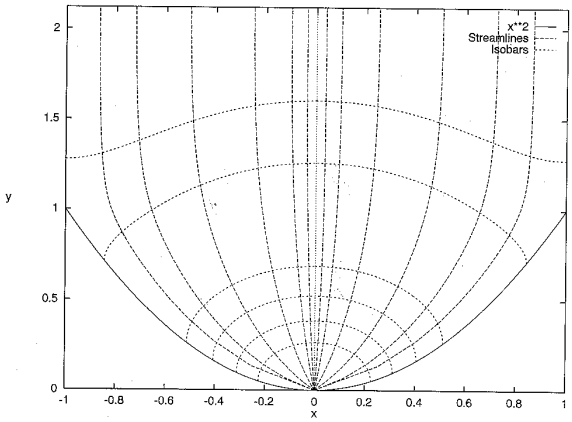

Figure 2. The computed streamlines and isobars in a bin with bottom shape as $y = x^2$.

in a Silicon-Graphics computer and we tested and found that the computation times are below two minutes for $y = x^2, x^4$ and x^8 with $M = 80$. As the system of equations in (5.10) is solved, the real and imaginary parts of (5.8), together with (5.6) and (5.7), then give the shapes of isobars and streamlines, respectively. A test for a direct check of the numerical results of the value of flow angle $\theta(\xi_j)$ was carried out, for the bottom shape function $y = x^2$. For increasing fineness $M = 40, 80, 120$ and 140, the solution of (5.10) shows satisfactory convergence in view of the error $O(h^2)$. The computed examples of streamlines and isobars are shown in Figures 2, 3 and 4 for $y = x^2, x^4$ and x^8, respectively. It is found that the closer the streamline are to the wall, the more grid points are required. In our computation, for instance, the streamlines starting with $C_2 = -0{\cdot}2$ and $0{\cdot}2$ the closest to bottom, for the solid wall $y = x^4$, 140 mesh points are chosen. The other streamlines are chosen from $C(i+1) = C(i) \pm (0{\cdot}2 + 0{\cdot}15e^{i-0{\cdot}15}), i = 1, \ldots, 5$ with $C(1) + C_1$. The isobars are computed from $C(j+1) = C(i) + 0{\cdot}125, j = 1, \ldots, 5$ with $C(1) = C_2 = 0{\cdot}22$ the one nearest to the source. The comparison of airflow streamlines in these three different bottom bins shows the influences of the shape of the wall on the steamlines. In the case of $y = x^2$, there is still some region of cereals around points at $(\pm 1, 1)$ where airflow goes through slowly and, as the shape of the wall changes from $y = x^2$ to $y = x^4$ and $y = x^8$, the area of such a region diminishes. The singularities at $x = \pm 1$, however, also affect the accuracy of the computed results as the isobars approach to the points $(\pm 1, 1)$. In the case of $y = x^8$ we also computed two more isobars above $y = 1$ showing the asymptotic behaviors.

6. Temperature distribution in a drying system

A temperature change occurs quite regularly in such a drying storage system. Since the convective effect is considered to be important during the process, the heat conduction equation is coupled with velocity in both the horizontal and the vertical directions. Even if the fluid field is in a steady state, finding an analytical solution for such an equation is not a trivial task. However, we may simplify this problem using the classic complex transformation, mapping the physical region into a complex potential plane. The heat-conduction equation is then reduced to an equation of the temperature distribution in terms of stream function and pressure.

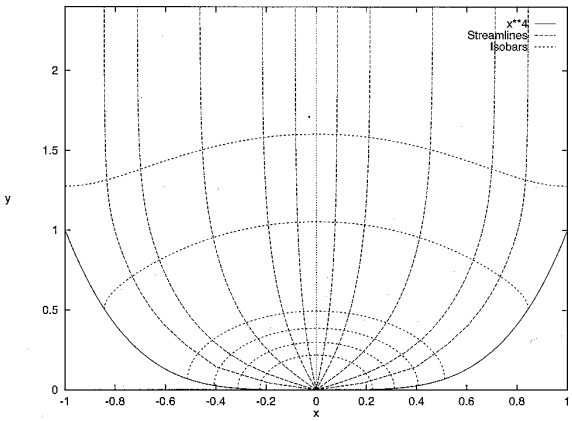

Figure 3. The computed streamlines and isobars in a bin with bottom shape as $y = x^4$.

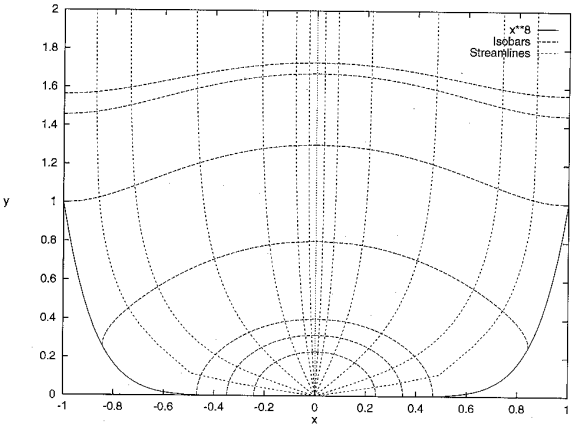

Figure 4. The computed streamlines and isobars in a bin with bottom shape as $y = x^8$.

6.1. HEAT CONDUCTION EQUATION ON THE COMPLEX POTENTIAL PLANE

The physical region can be transformed to a reference plane, say, the complex potential plane which has been studied in previous sections.

Two components of flow velocity **u** in terms of ϕ and ψ are as follows,

$$u = \phi_x = \psi_y, \qquad v = \phi_y = -\psi_x, \tag{6.1}$$

where $q^2 = |\mathbf{u}|^2 = u^2 + v^2$.

After changing variables x and y to ϕ and ψ, we have

$$\frac{\partial T}{\partial x} = \frac{\partial T}{\partial \phi}\frac{\partial \phi}{\partial x} + \frac{\partial T}{\partial \psi}\frac{\partial \psi}{\partial x}, \qquad \frac{\partial T}{\partial y} = \frac{\partial T}{\partial \phi}\frac{\partial \phi}{\partial y} + \frac{\partial T}{\partial \psi}\frac{\partial \psi}{\partial x}. \tag{6.2, 6.3}$$

Substituting these transformations in the left-hand side of (2.7), we have

$$\begin{aligned} u\frac{\partial T}{\partial x} + v\frac{\partial T}{\partial y} &= \left(u\frac{\partial \phi}{\partial x} + v\frac{\partial \phi}{\partial y}\right)\frac{\partial T}{\partial \phi} + \left(u\frac{\partial \psi}{\partial x} + v\frac{\partial \psi}{\partial y}\right)\frac{\partial T}{\partial \psi} \\ &= (u^2 + v^2)\frac{\partial T}{\partial \phi} + (-uv + vu)\frac{\partial T}{\partial \psi} = q^2\frac{\partial T}{\partial \phi}. \end{aligned} \tag{6.4}$$

Similarly, the right-hand side of (2.7) becomes

$$\frac{\partial^2 T}{\partial x^2} + \frac{\partial^2 T}{\partial y^2} = \left(\frac{\partial^2 T}{\partial \phi^2} + \frac{\partial^2 T}{\partial \psi^2}\right) q^2. \tag{6.5}$$

Then substituting Equations (6.4) and (6.5) in (2.7), we arrive at

$$\frac{\partial T}{\partial \phi} = \frac{1}{\mathrm{Pe}} \left(\frac{\partial^2 T}{\partial \phi^2} + \frac{\partial^2 T}{\partial \psi^2}\right). \tag{6.6}$$

Equation (6.6) is considerably simpler to solve, and standard techniques may be employed. Moreover, for the insulated boundary condition along impermeable walls $\psi = \pm 1$, after using Equations (6.2) and (6.3) we can show that

$$\frac{\partial T}{\partial \mathbf{n}} = 0 \Leftrightarrow \frac{\partial T}{\partial \psi} = 0.$$

This insulated boundary condition, together with another constant boundary condition, is investigated in the following section.

6.2. A SOLUTION OF THE HEAT-CONDITION EQUATION

We seek a solution of the reduced steady heat conduction Equation (6.6) with boundary conditions on the complex potential plane, which is a strip with two parallel lines $\psi = \pm 1$ as its boundaries, where $\psi = -1$ corresponds to $\widehat{AO}$, $\psi = 1$ to $\widehat{OD}$ (Figure 1(c)). However, we are more interested in the bins with finite height, which correspond to the semi-strip with $-\infty < \phi \leqslant \phi_0$ in the complex potential plane. From the analysis and numerical results in Section 5, we show that if constant ϕ_0 is chosen relatively, large, we will have $\phi \sim y + c_0$ and $\psi \sim x$. For instance, for the bin in Example 1 in Section 4, we have $|\phi - (y + \log 2)| < \mathrm{e}^{-\pi y} + 1/\sinh^2(\pi y/2)$, which is less than $7{\cdot}54 \times 10^{-7}$ when we choose $y = 5$. This shows that taking $\phi = \phi_0$ as the top of the bins changes very little the physical scenario.

We now use a separated-variable method to solve Equation (6.6). Substitution of

$$T(\phi, \psi) = T_1(\phi) T_2(\psi)$$

yields

$$T_1''(\phi) - \mathrm{Pe}\, T_1'(\phi) - K T(\phi) = 0, \qquad T_2''(\psi) + K T_2(\psi) = 0. \tag{6.7, 6.8}$$

To satisfy the boundary conditions (6.11), we let $T_2(\psi) = \cos p\pi\psi$, which is substituted in (6.8) to obtain $K = (p\pi)^2$. Replacing $K = (p\pi)^2$ in (6.7) and then trying $T_1(\phi) = \mathrm{e}^{\lambda\phi}$ yields an algebraic equation

$$\lambda^2 - \mathrm{Pe}\,\lambda - (p\pi)^2 = 0, \tag{6.9}$$

where λ_1 corresponds to positive sign '+' and λ_2 to negative sign '−'. The two roots of this equation are

$$\lambda_{1,2}(p) = \frac{\mathrm{Pe} \pm (\mathrm{Pe}^2 + 4(p\pi)^2)^{\frac{1}{2}}}{2} \tag{6.10}$$

Case 1. The boundary conditions are considered as follows

$$\frac{\partial T}{\partial \psi} = 0, \qquad \text{on} \quad \psi = \pm 1, \tag{6.11}$$

$$T \to 1 \quad \text{as} \quad \phi \to -\infty, \qquad T = f(\phi) \quad \text{on} \quad \phi = \phi_0. \tag{6.12}$$

A solution is constructed as

$$T(\phi, \psi) = 1 + \sum_{n=0}^{+\infty} a_n \, \mathrm{e}^{\lambda_1(n)\phi} \cos n\pi\psi. \tag{6.13}$$

Using the condition $T = f(\psi)$ on $\phi = \phi_0$, we find

$$a_n = \mathrm{e}^{-\lambda_1(n)\phi_0} \int_{-1}^{1} f(\psi) \cos n\pi\psi \, \mathrm{d}\psi.$$

Because of symmetry, $f(\psi)$ is an even function. We then have

$$a_n = 2\mathrm{e}^{-\lambda_1(n)\phi_0} \int_{0}^{1} f(\psi) \cos n\pi\psi \, \mathrm{d}\psi. \tag{6.14}$$

In a special case of $T = 0$ on $\phi = \phi_0$ together with insulated boundary conditions and $T \to 1$ as $\phi \to -\infty$, we find a solution as

$$T = 1 - \mathrm{e}^{\mathrm{Pe}(\phi - \phi_0)}. \tag{6.15}$$

Case 2. With boundary conditions $T(\phi, \psi) = \pm 1$ on $\psi = \pm 1$, $T = f(\psi)$ at $\phi = \phi_0$ and $T \to 1$ as $\phi \to -\infty$, similarly, we can construct a solution as

$$T(\phi, \psi) = 1 + \sum_{n=0}^{+\infty} a_k \, \mathrm{e}^{\lambda_1(k)\phi} \cos k\pi\psi, \qquad \text{with} \quad k = n + \tfrac{1}{2} \tag{6.16}$$

where a_k can be determined as

$$a_k = 2\mathrm{e}^{-\lambda_1(k)\phi_0} \int_{0}^{1} f(\psi) \cos k\pi\psi \, \mathrm{d}\psi. \tag{6.17}$$

The solution (6.16) corresponding to different Peclet numbers is plotted in Figure 6. We choose $f(\psi) = 0{\cdot}5|\sin \pi\psi/2|$ in Equation (6.13) in case 1. We obtain the coefficients a_n as follows,

$$a_0 = -\left(1 - \frac{1}{\pi}\right) \mathrm{e}^{-\mathrm{Pe}_{\phi_0}}, \qquad a_n = -\frac{1}{\pi} \frac{2\mathrm{e}^{-\lambda_1(n)\phi_0}}{4n^2 - 1}, \qquad \text{with} \quad n = 1, 2, \ldots.$$

Then the solution is written as

$$T(\phi, \psi) = 1 - \left(1 - \frac{1}{\pi}\right) \mathrm{e}^{\mathrm{Pe}_{(\phi - \phi_0)}} - \sum_{n=0}^{\infty} \frac{\cos n\pi\psi}{\pi} \frac{2\mathrm{e}^{\lambda_1(n)(\phi - \phi_0)}}{4n^2 - 1}, \tag{6.18}$$

which is truncated at $n = 3$ and plotted in Figure 5. Similarly, in case 2, we choose $f(\psi) = |\psi|$ and ψ^2. We obtain

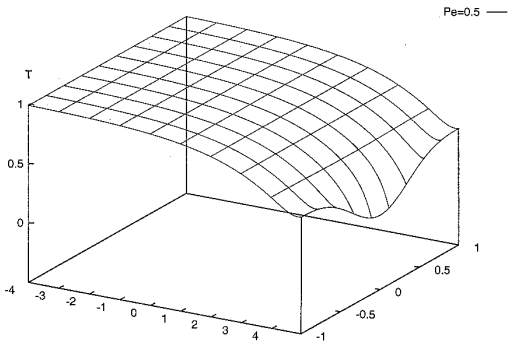

Figure 5. The temperature distribution of Equation (6.18) with $f(\psi) = 0{\cdot}5|\sin\frac{\pi\psi}{2}|$.

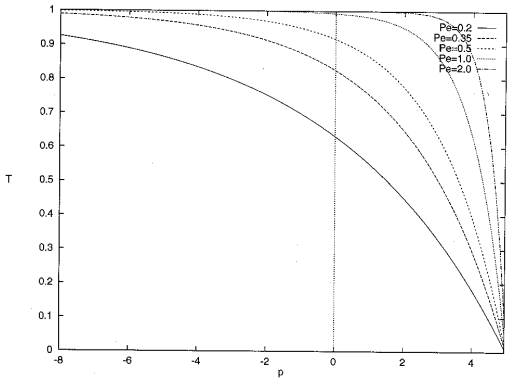

Figure 6. The temperature distributions for (6.16).

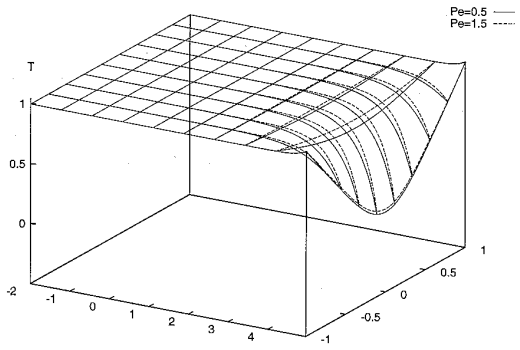

Figure 7. The temperature distributions for $f(\psi) = |\psi|$ with Pe $= 0{\cdot}5$ and $1{\cdot}5$ in Equation (6.19).

$$T(\phi, \psi) = 1 - \sum_{n=0}^{\infty} \frac{2e^{\lambda_1(n+1/2)(\phi-\phi_0)}}{((n+1/2)\pi)^2} \cos((n+1/2)\pi\psi) \tag{6.19}$$

and

$$T(\phi, \psi) = 1 + \sum_{n=0}^{\infty} (-1)^{n+1} \frac{4e^{\lambda_1(n+1/2)(\phi-\phi_0)}}{((n+1/2)\pi)^3} \cos((n+1/2)\pi\psi), \tag{6.20}$$

respectively. The function in (6.19) is truncated at $n = 4$ and plotted with Pe $= 0{\cdot}5$ and $1{\cdot}5$, shown in Figure 7.

Conclusions

This work presents a treatment of solving airflow fields within bins for different geometries and temperature distributions of fluid in these bins. Using a generalized Schwarz-Christoffel formula, we transformed the physical region to a reference plane and then reduced the problem to a single nonlinear equation. After solving this equation numerically, we showed the effect of changing the bottom shapes of bins on streamlines and isobars of airflow. The computation is comparatively simple. The heat-conduction equation is changed into an equation in terms

of stream function and complex potential. Analytical solutions have been found for the steady state temperature in the bins with different boundary conditions. Future work will incorporate the effect of the interaction between the moisture of the grain and the humidity of the air. It will be also interesting to expand this work to high-speed nonlinear flows.

Acknowledgement

The authors are very grateful to the referees for their valuable comments and suggestions. We also would like to thank one of the referees for pointing out the work of Jordinson and Wooding.

References

1. H. B. Spencer, Pressure drop in on-floor duct drying systems. *J. Agric. Eng. Res.* 14 (1969) 165–172.
2. A. J. Hunter, Pressure difference across aerated seed bulk for some common duct and store cross-section. *J. Agric. Eng. Res.* 28 (1983) 437–450.
3. J. M. Goudie, E. A. Smith and A. de Ville, Modelling velocity of air through beds of cereal grains. *IMA J. Math. Appl. in Bus. & Ind.* 5 (1995) 325–335.
4. E. A. Smith, Pressure and velocity of air during drying and storage of cereal grains. *Transport in Porous Media* 23 (1996) 197–218.
5. S. Ergun, Fluid flow through packed columns. *Chem. Eng. Prog.* 48 (1952) 89–94.
6. British Ministry of Agriculture, Fisheries and Food, Bulk Grain Driers. *Booklet 2416* (1982).
7. R. Jordinson, Design of wind tunnel contractions. *Aircr. Engr. Lond.* 33 (1961) 294–297.
8. R. W. Wooding, A low-speed wind tunnel for model studies in micro-meteorology. *Div. Plant. Ind. Tech. Pap.* 25 (1968) CSIRO Melbourne Australia.
9. L. C. Woods, *The Theory of Subsonic Plane Flow*, Cambridge University Press (1961) 594pp.
10. M. I. G. Bloor, Large amplitude surface waves. *J. Fluid Mech.* 84 (1978) 167–179.
11. A. C. King and M. I. G. Bloor, Free surface flow over a step. *J. Fluid Mech.* 182 (1987) 193–208.
12. W. V. Hukill and C. K. Shedd, Nonlinear airflow in grain drying. *Agr. Eng.* 36 (1955) 462–466.
13. E. A. Smith, D. S. Jayas, W. E. Muir, K. Alagusundaram and V. H. Kalbande, Simulation of grain drying in bins with partially perforated floors. *Trans. Am. Soc. Agr. Eng.* 35 (1992) 909–915.